Inversion of polar motion data: Chandler wobble, phase jumps, and geomagnetic jerks

Dominique Gibert, Jean-Louis Le Mouël

Inversion of polar motion data: Chandler wobble, phase jumps, and geomagnetic jerks

Dominique Gibert[1] and Jean-Louis Le Mouël[1]

Received 18 March 2008; revised 11 July 2008; accepted 24 July 2008; published 23 October 2008.

[1] We reconsider the analysis of the polar motion with a method totally different from the wavelet analysis used in previous papers. The total polar motion is represented as the sum of oscillating annual and Chandler terms whose amplitude and phase perturbations are inverted with a nonlinear simulated annealing method. The phase variations found in previous papers are confirmed with the huge phase change ($\approx 3\pi/2$) occurring in the 1926–1942 period and another less important one ($\approx \pi/3$) in the 1970–1980 epoch. The best Chandler period, T_c, is found to be 434 ± 0.5 mean solar days. The epochs of significant phase changes found in the Chandler wobble are also those where important geomagnetic jerks occur in the secular variation of the geomagnetic field. Turbulent viscous friction produced by small-scale topography at the core-mantle boundary might be responsible for the observed phase jumps.

Citation: Gibert, D., and J.-L. Le Mouël (2008), Inversion of polar motion data: Chandler wobble, phase jumps, and geomagnetic jerks, *J. Geophys. Res.*, *113*, B10405, doi:10.1029/2008JB005700.

1. Introduction

[2] The movement of the Earth's pole has been observed for more than 150 years, and, at the end of the 19th century, *Chandler* [1891a, 1891b] showed that this motion is the sum of two periodic oscillations, the forced annual oscillation and the Chandler wobble with a period close to 434 mean solar days [e.g., *Guinot*, 1972; *Lambeck*, 1980; *Wahr*, 1988; *Cazenave and Feigl*, 1994]. Both the amplitude and the phase of the Chandler wobble vary with time [e.g., *Lambeck*, 1980], and *Danjon and Guinot* [1954] first reported a phase change of about 150° which occurred around 1926 and was achieved in less than 10 years [*Guinot*, 1972]. This phase jump remained poorly documented until other jumps were reported by *Gibert et al.* [1998] and suggested to be in temporal coincidence with geomagnetic jerks [*Gibert et al.*, 1998; *Bellanger et al.*, 2002]. Similar phase jumps have been detected in the Free Core Nutation time series and also found in coincidence with geomagnetic jerks [*Shirai et al.*, 2005].

[3] Different hypotheses have been proposed as the excitation mechanism of the Chandler wobble (see *Dehant and de Viron* [2002] for a short review), the main ones being the atmosphere [e.g., *Aoyama and Naito*, 2001], the pressure at the bottom of the oceans [*Gross*, 2000; *Brzeziński and Nastula*, 2002; *Gross et al.*, 2003], the earthquakes [*Mansinha and Smylie*, 1967; *Gross*, 1986], or core motions [*Wahr*, 1988; *Dickman*, 1993]). The proposed temporal coincidence between geomagnetic jerks and phase jumps in the Chandler wobble constitutes an exciting challenge and constitutes a new clue to the role of core-mantle coupling onto the Earth's polar motion.

[4] In the present paper, we reconsider the analysis of the Earth's polar motion with a new method totally different from the wavelet analysis used in our earlier papers [*Gibert et al.*, 1998; *Bellanger et al.*, 2002]. Also, the inverse approach followed in the present study is more direct in the sense that the detrended total polar motion is analyzed without the complicated preprocessing stages of the wavelet analysis. Moreover, we hope this new and simpler method will be more easily used by independent teams in order to perform analysis similar to the one presented here.

[5] In the remaining of the present paper, we first present the polar motion series and describe the model used to compute realistic synthetic series to be compared with the data. Then, we detail the parameterization of the inverse problem where the amplitudes of the annual and Chandler components of the polar motion are to be retrieved together with the phase curve of the Chandler term. Next, the nonlinear inversion is performed with the simulated annealing method and a Bayesian assessment of the uncertainty attached to the estimated parameters is done with the Metropolis algorithm.

2. Modeling of the Polar Motion

2.1. Polar Motion Data

[6] The total polar motion, $m(t)$, provided by the International Earth Rotation Service (IERS) (data series eopc01) is shown in Figure 1a. Let us recall that the coordinate system is left-handed with the X axis coinciding with the Greenwich meridian and the Y axis corresponding to the $W90$ meridian. This signal is the superimposition of a smooth secular drift $d(t)$ and of an oscillating term $o(t)$ resulting from interferences between the annual prograde and retrograde components, $a_p(t)$ $a_r(t)$, and the prograde Chandler

[1]Institut de Physique du Globe, CNRS/INSU UMR 7154, Paris, France.

0148-0227/08/2008JB005700$09.00

wobble $c(t)$ [*Lambeck*, 1980]. In previous studies [*Gibert et al.*, 1998; *Bellanger et al.*, 2002], we showed that the annual prograde component is dominant with respect to the retrograde one which, however, remains significant (see the inset in Figure 2c for an illustration of the importance of the retrograde annual component). In the same studies, it was also shown that the Chandler wobble is affected by a small number of phase perturbations $\Delta\phi(t)$ whose temporal shape may be modeled as sigmoid phase jumps with a short duration of the order of one year. Accounting for these observations the total polar motion may be written as,

$$\begin{aligned} m(t) &= o(t) + d(t) + n(t) \\ &= a_p(t) + a_r(t) + c(t) + d(t) + n(t), \end{aligned} \tag{1}$$

where $n(t)$ represents the noise presents in the data (Figure 1c).

[7] In the present study we remove the secular drift before inverting the data. Owing to the smooth nature of $d(t)$, we represent it by the least squares fitted polynomials of degree 5 shown in Figure 1a. No significant differences were observed when using either fourth and sixth degree polynomials. The noisy oscillating part, $o(t) + n(t)$, is obtained by subtracting the fitted polynomials from the total polar motion and is shown in Figure 1b.

[8] We remark that IERS data at face value, and the polar motion series shown in Figure 1a results from the merging of series with data of different nature (for more details, see IERS Web site http://www.iers.org). For instance, it cannot be eliminated that some inconsistencies affect the data in the 1970–1980 period due to the merging of classical astrometric and space geodetic measurements [*Gross and Vondrák*, 1999].

2.2. Parameterization of the Polar Motion Model

[9] The signal to be inverted is the $o(t)$ part of the total polar motion and, in the present study, the model of signal used in the forward problem reads,

$$\begin{aligned} o^m(t) = {} & A_{pa}(t) \exp\left[\frac{2i\pi t}{T_a} + i\Delta\phi_{pa}\right] \\ & + A_{ra}(t) \exp\left[-\frac{2i\pi t}{T_a} - i\Delta\phi_{ra}\right] \\ & + A_c(t) \exp\left[\frac{2i\pi t}{T_c} + i\Delta\phi(t)\right], \end{aligned} \tag{2}$$

where the real amplitudes $A_{pa}(t)$, $A_{ra}(t)$, $A_c(t)$, the phase variation $\Delta\phi(t)$, and the constant phase shifts $\Delta\phi_{pa}$, $\Delta\phi_{ra}$ of the annual components are to be determined. The period T_a = 365.25 mean solar days (msd) and the Chandler period T_c is assumed known and constant during a given inversion. The Chandler period is not considered as a parameter to be inverted since the phase variation $\Delta\phi(t)$ may incorporate a period change δT_c through the linear correcting term,

$$\Delta\phi(t) = -\frac{2\pi t}{T_c} \times \frac{\delta T_c}{T_c + \delta T_c}. \tag{3}$$

Equation (3) shows that a change in the choice of the Chandler period T_c will result in a change in the linear drift of the phase $\Delta\phi$ (see discussion below).

[10] As can be seen in equation (2), the amplitudes are linear parameters, while the phase variation is a nonlinear one. In what follows, the inversion will not deal directly with these unknown functions, but instead will be performed for primary parameters from which the $A_{pa}(t)$, $A_{ra}(t)$, $A_c(t)$ and $\Delta\phi(t)$ functions are deduced. More explicitly, the amplitude functions are obtained by linearly interpolating coarsely sampled amplitude functions. In practice, this reads

$$A_{pa}(t) = \mathcal{LI}\left[\left(A_{pa,1}, t_1\right), \cdots, \left(A_{pa,k}, t_k\right), \cdots, \left(A_{pa,N}, t_N\right)\right], \tag{4}$$

$$A_{ra}(t) = \mathcal{LI}\left[\left(A_{ra,1}, t_1\right), \cdots, \left(A_{ra,k}, t_k\right), \cdots, \left(A_{ra,N}, t_N\right)\right], \tag{5}$$

$$A_c(t) = \mathcal{LI}\left[\left(A_{c,1}, t_1\right), \cdots, \left(A_{c,k}, t_k\right), \cdots, \left(A_{c,N}, t_N\right)\right], \tag{6}$$

where $\mathcal{LI}$ represents the linear interpolation operator, and where the dates t_k are fixed and regularly distributed with a sampling interval of 3 months. Consequently, for amplitudes, the parameters to be actually determined are the elements of the three sets $\{A_{pa,k},\ k = 1, N\}$, $\{A_{ra,k},\ k = 1, N\}$, and $\{A_{c,k},\ k = 1, N\}$.

[11] An identical parameterization is adopted for the phase variation function $\Delta\phi(t)$,

$$\Delta\phi(t) = \mathcal{LI}\left[\left(\Delta\phi_1, t'_1\right), \left(\Delta\phi_2, t'_2\right), \cdots, \left(\Delta\phi_k, t'_k\right), \cdots, \left(\Delta\phi_M, t'_M\right)\right] \tag{7}$$

with the important difference that the dates t'_k are not fixed but, instead, are to be determined together with the phase variations $\Delta\phi_k$. This parameterization makes the inversion highly non linear but, as will be seen later, it permits us to eventually represent the phase function with a very small number M of parameters.

[12] To summarize, the model to be determined is the set of parameters,

$$\begin{aligned} \mathcal{M} = {} & \left\{A_{pa,1}, \cdots, A_{pa,k}, \cdots, A_{pa,N}\right\} \\ & \bigcup \left\{A_{ra,1}, \cdots, A_{ra,k}, \cdots, A_{ra,N}\right\} \\ & \bigcup \left\{A_{c,1}, \cdots, A_{c,k}, \cdots, A_{c,N}\right\} \\ & \bigcup \left\{\Delta\phi_1, \cdots, \Delta\phi_k, \cdots, \Delta\phi_M\right\} \\ & \bigcup \left\{t'_1, \cdots, t'_k, \cdots, t'_M\right\} \\ & \bigcup \left\{\Delta\phi_{pa}, \Delta\phi_{ra}\right\}, \end{aligned} \tag{8}$$

from which the functions $A_{pa}(t)$, $A_{ra}(t)$, $A_c(t)$ and $\Delta\phi(t)$ are deduced. We determine these parameters through a two-step procedure by, first, searching for a good model fitting with the data, and, second, exploring the nonuniqueness of the solution. The first step is accomplished by using a global search method, namely simulated annealing, and the second step uses a heat bath method based on the Metropolis algorithm as explained in the sections 3 and 4.

3. Inversion by Simulated Annealing

3.1. Method

[13] The search for a good model, $\mathcal{M}_{\text{best}}$, is done with the simulated annealing algorithm which allows us to easily

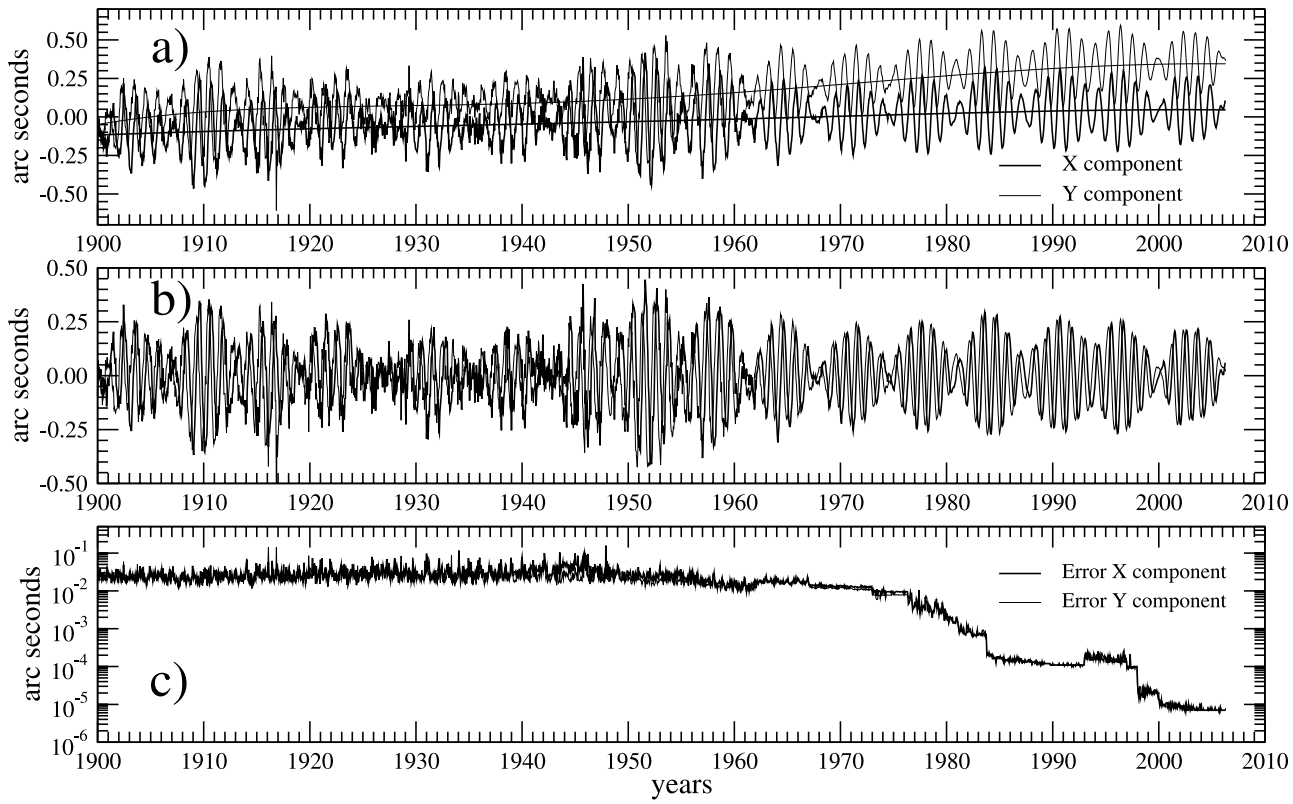

Figure 1. Polar motion data. (a) Total polar motion series eopc01 provided by the International Earth Rotation Service, the X and Y components correspond to the thick and thin lines, respectively. Also shown are the order 5 polynomials representing the smooth secular drift, $d(t)$, of the pole. (b) The oscillating polar motion, $o(t)$, obtained by subtracting the order 5 polynomials from the original series, $m(t)$, shown in Figure 1a. (c) The IERS's estimate of the noise level for the original series. A logarithmic scale must be used for the ordinate axis in order to account for the huge reduction of the noise during the 20th century. For comparison with the signals shown above, average values of the error are 0.025 arc sec before 1960 and 0.012 arc sec in 1960–1970 period. The dramatic decrease of the noise level which initiates in 1976 is due to the incorporation of space geodetic measurements into the polar motion time series [*Gross and Vondrák*, 1999].

deal with nonlinear models and sophisticated likelihood functions. In the following, we shall only give the technical details specifically adjusted for the present study, and the reader is referred to *Metropolis et al.* [1953], *Kirkpatrick et al.* [1983], *Bhanot* [1988], and *Sambridge and Mosegaard* [2002] for general considerations concerning the Metropolis and the simulated annealing algorithms in the framework of nonlinear inversion.

[14] In what follows, the likelihood function used to assess for the quality of a model $\mathcal{M}$ is taken Gaussian-like,

$$L(\mathcal{M}) = \exp\left[-\|o(t) + n(t) - o^m(t)\|^2\right], \tag{9}$$

where $||\cdot||^2$ represent the L^2 norm of a vector. For the moment, this likelihood function does not need to be either scaled or normalized as it will serve only to quantify the relative goodness of fit of the models.

[15] Simulated annealing consists in a sequence of Metropolis loops while simultaneously applying a topological transformation to the likelihood L by decreasing a control parameter T traditionally called the temperature [*Kirkpatrick et al.*, 1983; *Gibert and Virieux*, 1991; *Mosegaard and Tarantola*, 1995; *Pessel and Gibert*, 2003]. The transformed likelihood is given by,

$$L_T(\mathcal{M}) = L^{1/T}(\mathcal{M}). \tag{10}$$

The simulated annealing begins with $T \to \infty$ for which L_∞ equals a constant and stops at either $T = 1$ when the likelihood is the one given by equation (9) or at $T \approx 0$ with $L_0 \approx \delta\ (\mathcal{M}_{\text{best}} - \mathcal{M})$ where $\mathcal{M}_{\text{best}}$ is the searched best fitting model (i.e., $L(\mathcal{M}_{\text{best}}) > \mathcal{M}$). For each temperature T, a Metropolis loop produces a sequence of models distributed according to L_T. In practice, this consists in generating a sequence of models where the next model, $\mathcal{M}^{j+1}$, to be added in the sequence is obtained from the preceding one, $\mathcal{M}^j$, according to the random choice,

$$\text{prob}\left[\mathcal{M}^{j+1} = \mathcal{M}^{\text{try}}\right] = \min\left[1, \frac{L_T(\mathcal{M}^{\text{try}})}{L_T(\mathcal{M}^j)}\right], \tag{11}$$

where $\mathcal{M}^{\text{try}}$ is a candidate model to be eventually included in the sequence of models. Equation (11) indicates that a

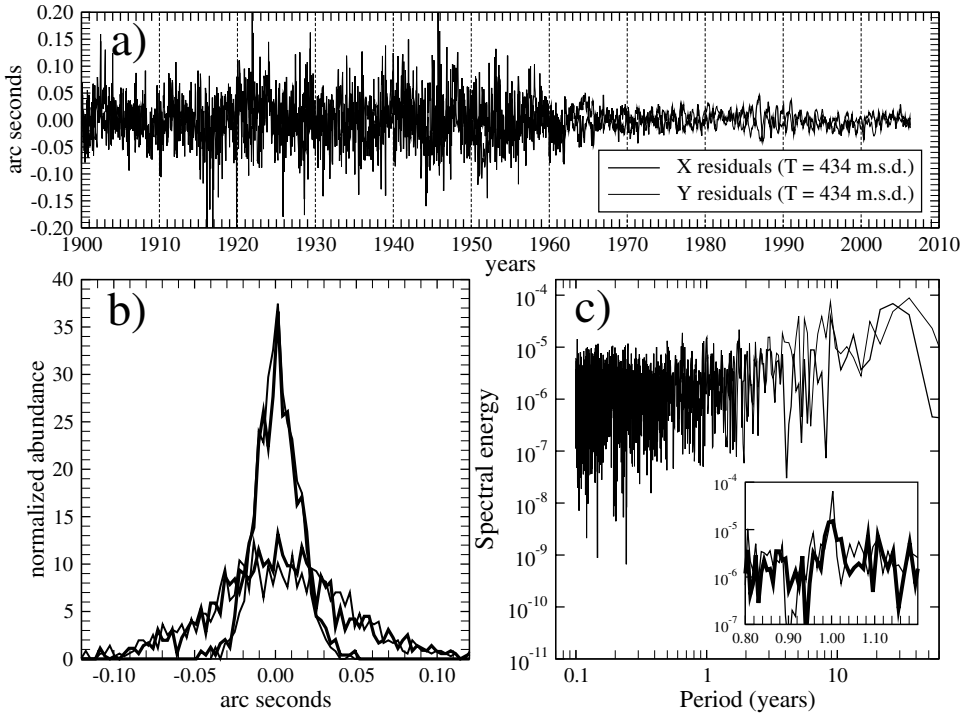

Figure 2. (a) Residuals (data minus synthetics) for the X and Y components obtained for the model fitted with T_c = 434 msd. (b) Histogram of the residuals: the wide histograms correspond to the residuals before 1960 (SD = 0.04435), and the narrow histograms are for the residuals after 1965 (SD = 0.01426). Thick and thin curves are for the X and Y components respectively. (c) Energy spectrum of the residuals for the X (thick curve) and Y (thin curve) components; inset is magnification of the spectra of the X component for residuals of models with (thick line) and without (thin line) the retrograde annual component. The same result is observed for the Y component.

more likely model is always accepted and that a less likely model is sometimes accepted. When the random assignment given by equation (11) fails, i.e., when the less likely candidate model has been rejected, the replicating transition $\mathcal{M}^{j+1} = \mathcal{M}^j$ is applied. As the Metropolis loop proceeds, a sequence of models is generated such that more models fall in the most likely regions of the model space. When the temperature decreases, these regions have their likelihood dramatically (i.e., exponentially) augmented, and if the temperature is slowly lowered, the chain of models is gently guided toward the regions of the model space where the likelihood is maximum [*Metropolis et al.*, 1953; *Bhanot*, 1988].

[16] The candidate model, $\mathcal{M}^{\text{try}}$, is obtained by perturbing the current model $\mathcal{M}^j$ in order to give some memory to the Metropolis chain. This point is particularly important since it makes the algorithm not a simple Monte Carlo search. In the present study, we observed that the perturbation strategy is not a critical matter, and the method we retained consists in randomly choosing the parameters to be perturbed in the parameter set $\mathcal{M}^j$.

[17] The perturbation applied to the amplitudes $A_{pa,k}$, $A_{ra,k}$, $A_{c,k}$ is randomly assigned with the following rule:

$$A^{\text{try}}_{.,k} = A^{j}_{.,k} + \text{rand}_1[-0.02 \text{ arc sec}, +0.02 \text{ arc sec}], \tag{12}$$

where $\text{rand}_\alpha[x_1, x_2]$ represents the biased uniform random generator in the $[x_1, x_2]$ interval with the probability $1 - \alpha$ that the random generator returns a zero value. The phase variation is perturbed by randomly drawing a parameter $\Delta\phi_k$ in $\mathcal{M}^j$ and perturbing it with the rule,

$$\Delta\phi^{\text{try}}_k = \Delta\phi^j_k + \text{rand}_{0.5}[-30^\circ, +30^\circ]. \tag{13}$$

The corresponding date, t'_k, is also modified according to,

$$t'^{,\text{try}}_k = t'^{,j}_k + \text{rand}_{0.5}[-0.75 \text{ year}, +0.75 \text{ year}]. \tag{14}$$

[18] Observe that the random generator is biased in both equations (13) and (14), so that a drawn parameter is actually perturbed only half of the time. We found this rule necessary because of the very different roles played by the various parameters. We indeed observed that the phase parameters are more rapidly determined than the amplitude ones. A way to deal with this situation is to reduce the perturbation of the phase parameters which become determined first. The biased random generator provides a solution in the sense that no perturbation of both $\Delta\phi_k$ and t'_k occurs 25% of the time (equations (13) and (14)). Furthermore, the phase variations $\Delta\phi_k$ have quite a complicated contribution to the misfit budget, i.e., in the likelihood L, since those with dates falling at the beginning of the 20th century concern longer portions of signal than those place near the end of the century. When running the simulated annealing algorithm, we observed a hierarchical determination

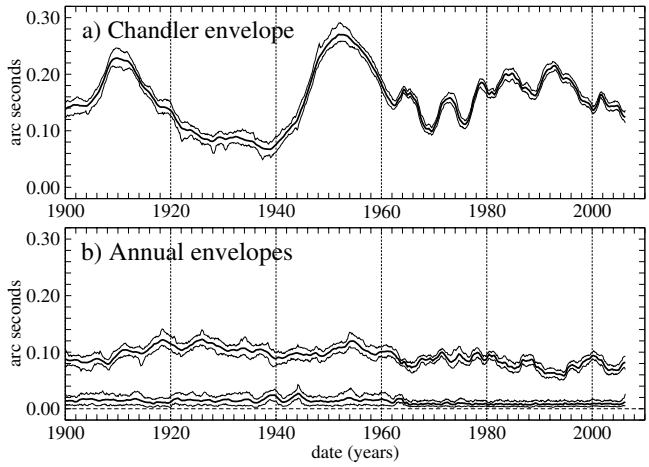

Figure 3. (a) Envelopes of the Chandler component, and (b) the prograde (top curves) and the retrograde (bottom curves) annual components obtained by inverting the detrended polar motion (Figure 1) T_c = 434 mean solar days. The thick curves are the envelopes of the average model of the models produced by Metropolis sequences, and the thin curves represent the extremes envelopes of all models accepted in these sequences. The horizontal dashed line represents the zero level in order to show that the retrograde annual amplitude remains significantly different from zero in the recent period where the data are more accurate.

of the parameters, with those placed at the beginning of the century being locked more quickly than those placed later.

[19] The temperature schedule, i.e., the manner by which the temperature T is lowered, must be carefully designed to obtain a successful convergence toward models with a high likelihood. In the present study, the main difficulty we encountered was related to the hierarchical importance among the parameters to be determined. In practice we observed that too rapid a cooling made the Metropolis sequences of models get trapped in local minimums located far from the best models. A detailed analysis of this difficulty revealed that the trapping was due to parameters associated with dates early in the century. Indeed, changing the value or the date of such parameters produced huge perturbations in the more recent part of the synthetic signals, resulting in a high misfit and, consequently, in a low probability. Since the lower the temperature, the lower the probability to accept a poorer model in the Metropolis sequence, the perturbations applied to the parameters placed early in the 20th century were always rejected, and the Metropolis sequence was unable to escape from the local minimum. This problem was solved by controlling the cooling with the constant thermodynamical speed algorithm already used by *Gibert and Virieux* [1991]. The main advantage of this algorithm is to automatically reduce the perturbations of the parameters when the convergence accelerates.

3.2. Results

[20] The starting temperature, T_{start}, of the simulated annealing must be large enough to ensure that $L_{T_{\text{start}}} \approx 1$ so that a global sampling of the model space is performed [*Kirkpatrick et al.*, 1983; *Mosegaard and Tarantola*, 1995] In the present study, we use $T_{\text{start}} = 1$ for which almost all models $\mathcal{M}^{\text{try}}$ (starting, for example, from a first model with a constant amplitude and a null phase) are accepted in the Metropolis sequence, and 20 trial models $\mathcal{M}^{\text{try}}$ were tested (and a fraction of them retained, see equation (11)) for each Metropolis sequence. The final temperature was taken as $T = 10^{-5}$. A total of 10^7 models were tested during the whole process, and several inversions were done with T_c = 431, 432, 433, 434, and 435 mean solar days. For these inversions, we set $M = 23$ and $N = 425$ (see equation (8)). A large value was chosen for N to ensure a good modeling of the envelopes of the signals and eliminate the possibility that a bad envelope modeling could produce phase perturbations. On the opposite, a rather small value was chosen for M in order to comply with the hypothesis that only a small number of phase impulses are present in the Chandler component. This strong hypothesis was relaxed inverting the most recent part of the polar motion series with a large M = 71 (see below).

[21] Figure 2a shows the residuals corresponding to the best fitting model obtained for $T_c = 434$ msd. Similar results were obtained for the other Chandler periods. The most conspicuous feature visible in Figure 2a is the dramatic reduction of the residuals level for $t \gtrapprox 1962$. Histograms of the residuals (Figure 2b) which give standard deviations of 0.04435 arc sec and 0.01426 arc sec before 1960 and after 1965, respectively. Note that the decrease of the amplitude of the residuals in 1962 coincides with the decrease of the noise starting in 1962 as estimated by IERS (Figure 1c). That means that the big residuals before 1962 (Figure 2b) was essentially noise for the largest part. Afterward, the IERS estimation of noise keeps decreasing strongly, a characteristics which is not reflected in our residuals. We have to conclude that signal remains in our residuals.

[22] Figure 2c shows the energy spectrum of the residuals of Figure 2a. This spectrum is reasonably white in its high-frequency domain and becomes more similar to a pink noise for periods greater than about 3 years. The inset in Figure 2c shows a comparison of the energy spectra of the residuals obtained for models with and without the retrograde annual component. It can be seen that the spectrum for the model without the retrograde annual term has a significant peak at the period of 1 year. This peak disappears in the spectrum corresponding to the model with the retrograde annual component. This result favors the use of a retrograde annual term in the fitted model (equation (2)).

4. Posterior Probability

4.1. Method

[23] The residuals obtained for the best fitting models found with the simulated annealing can now be used to perform a statistical Bayesian inversion. Indeed, the likelihood function given by equation (9) can be completed to obtain a normalized probability density function,

$$L(\mathcal{M}) = \beta \exp\left[-\frac{\|o(t) + n(t) - o^m(t)\|^2}{2\sigma^2}\right], \qquad (15)$$

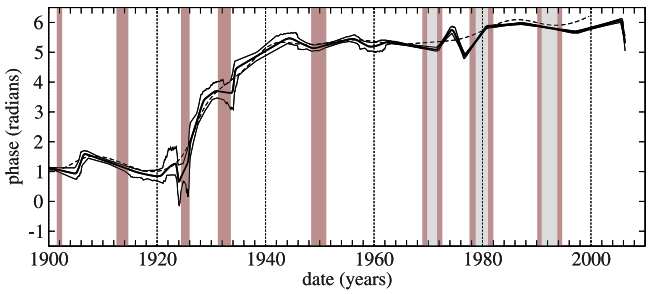

Figure 4. Phase variation, $\Delta\phi(t)$, inverted for T_c = 434 mean solar days. The thick curve is the phase curve of the average model of all models produced by a Metropolis sequence, and the thin curves represent the extreme envelopes of the models accepted during the sequence. The dashed curve represents the phase variation obtained by integrating the ridge function (i.e., the instantaneous frequency curve) of the Chandler prograde component shown in Figure 1 (top) of *Bellanger et al.* [2002]. The vertical bands represent the dates of occurrence of the geomagnetic jerks. The width of each band is tuned according to the dating uncertainties reported by *Alexandrescu et al.* [1995, 1996]. The multiple bands associated with the 1969, 1980, and 1991 jerks represent the bimodal nature of their occurrence date histograms [*Alexandrescu et al.*, 1996; *De Michelis and Tozzi*, 2005].

where β is a suitable normalizing constant and σ equals either 0.04435 arc sec or 0.01426 arc sec for t smaller or greater than 1962, respectively.

[24] As explained before, the Metropolis algorithm generates a sequence of models distributed according to the likelihood functions. So, by running a Metropolis loop for T = 1 and L given by equation (15), we obtain a set of acceptable models from which uncertainties may be computed. In practice, the computer code is the one used for the simulated annealing except that the starting model is the last one obtained in the simulated annealing inversion and that the temperature is maintained equal to 1. Let us also remark that the normalizing constant β in equation (15) has not to be computed in practice since it cancels in the likelihood ratio used in the Metropolis test (11).

4.2. Results

[25] Figure 3 shows the amplitudes $A_{pa}(t)$, $A_{ra}(t)$, and $A_c(t)$ interpolated from the model with T_c = 434 msd. The thick lines represent the average amplitudes for a Metropolis sequence of 10^6 models. The thin lines are the envelopes of the whole set of models accepted during the sequence. As expected, the envelopes are closer after 1962, when the noise level is smaller. Interestingly, at that date, the envelope of the retrograde annual component becomes smaller but with its lower envelope slightly above zero. At the same time, a clear decrease is observed in the prograde annual component amplitude which recovers a lower level similar to the one of the period 1900–1906.

[26] Figure 4 shows the phase variation, $\Delta\phi(t)$, interpolated from the model with T_c = 434 msd. Again, a reduction of the uncertainty domain is observed for $t \geq 1962$. Figure 5 shows the phase curves for T_c = 431, 432, 433, 434, and 435 mean solar days. All curves possess similar features but differ by the global drift of their linear segments where no significant phase jumps occur (e.g., the two segments corresponding to the horizontal arrows in Figure 4). Owing to the fact that a global linear drift may be due to a wrong choice for the value of T_c as shown by equation (3), the right period is the one for which these drifts are minimized. Accordingly, one can observe that the curve corresponding to T_c = 434 msd appears free of linear drift while those for T_c = 433 and 435 msd display a small but significant negative and positive drift, respectively. We conclude that the Chandler base period may be taken as $T_c = 434 \pm 0.5$ mean solar days in full agreement with our previous determination based on parsimony arguments [*Gibert et al.*, 1998].

[27] Another inversion restricted to $t \geq 1970$ was performed with a model counting a large number (M = 71) of parameters $\Delta\phi_k$ and t'_k. The resulting phase curve is shown in Figure 6; interestingly, we observe that this curve is very similar to the one obtained with a small number of parameters, confirming that the angular behavior of the phase variations is not due to modeling artifacts.

5. Discussion

[28] Let us write the Chandler wobble time series in the form

$$c(t) = A_c(t)\exp[i(\omega_c t + \phi(t))] = A_c(t)\exp\left[i\int_0^t (\omega_c + \delta\phi(\tau))\mathrm{d}\tau\right], \quad (16)$$

where $\omega_c = 2\pi/T_c$. The origin of time is taken at the beginning of the time series. The two above expressions are obviously strictly equivalent, with $\phi(t) = \int_0^t \delta\phi(\tau)\mathrm{d}\tau + \phi_0$, and $\delta\phi(t) = \phi'(t)$. It is also clear that changing ω_c or T_c comes down to adding a linear trend to $\phi(t)$: $\omega_c \rightarrow \omega_c + \delta\omega_c$, $\phi(t) \rightarrow \phi(t) - \delta\omega_c t$. For the reasons given above, we chose T_c = 434 (Figures 4, 5, and 6).

[29] Let us compare the phase variations shown in Figures 4 and 6 with our previous results [*Gibert et al.*, 1998; *Bellanger et al.*, 2002], i.e., the phase variation curve obtained by integrating the ridge function of the wavelet analysis of polar motion data [*Bellanger et al.*, 2002]. Figure 4 shows that the latter curve is in full general agreement with the phase variations obtained in the present study with a totally different method; however, the view of Figures 4, 5, and 6 reveals that the phase variations

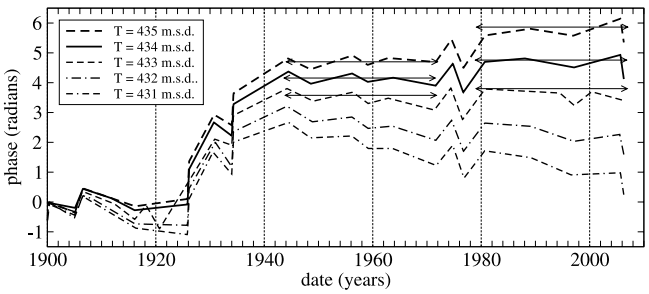

Figure 5. Phase variation $\Delta\phi(t)$ evolution of the $\mathcal{M}_{\mathrm{best}}$ models obtained for five reference periods T_c = 431, 432, 433, 434, and 435 mean solar days.

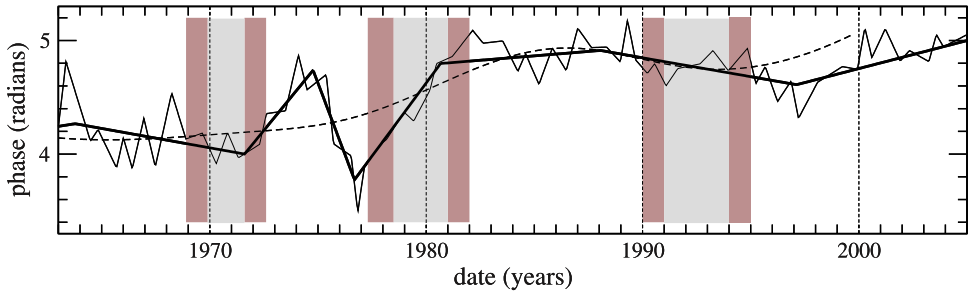

Figure 6. The thin solid line represents the phase variation, $\Delta\phi(t)$, inverted for a reference period T_c = 434 mean solar days and for a large number M = 71 of pilot points. The thick solid line represents the phase curve inverted for a small number (M = 9 in the represented time interval) of pilot points (Figure 5). The dashed curve represents the phase variation obtained by integrating the ridge function (i.e., the instantaneous frequency curve) of the Chandler prograde component shown in Figure 1 (top) of *Bellanger et al.* [2002]. The vertical bands represent the dates of the recognized geomagnetic jerks (see caption of Figure 4 for details).

recovered in the present paper appear sharper than the smooth curve obtained by wavelet analysis, which does not display by construction [see *Gibert et al.*, 1998, Figure 7], the segmented nature of the phase variations. Note that this segmented nature of the curve of the present study (Figure 5) is not an effect of the algorithm characteristics since the main pattern is preserved in the high-resolution inversion of Figure 6; it mean that the $o(t)$ data presents important phase variations at discrete times. The last increasing part of the integrated curve starts in 1994, while only in 1997 for the curves obtained in the present study. This discrepancy is probably due to a small edge effect in the wavelet analysis.

[30] Let us come back to the analysis of *Gibert et al.* [1998] and *Bellanger et al.* [2002]. In this paper we located phase jumps near the dates of geomagnetic jerks determined from geomagnetic observatory series, and we adjusted the amplitudes and durations of the phase jumps, supposed to have a sigmoid shape, in such a way that the phase curves determined from this modeling be identical to the integrated ridge function obtained from the data by wavelet analysis. The close similarity between the phase curve obtained in the present paper and the one computed earlier buttresses of our former analysis (i.e., locating phase jumps at the jerks time).

[31] Geomagnetic jerks are short-duration events which punctuate the evolution of the fluid core motion at the core-mantle boundary (CMB); such events have been detected in 1901, 1926, 1932, 1949, 1969, 1980 [*Alexandrescu et al.*, 1995, 1996], and 1991 [*Macmillan*, 1996; *De Michelis and Tozzi*, 2005]. The time of occurrence of a jerk is not determined with a high accuracy for two main reasons: (1) the (weak) conductivity of the mantle smooths out the shortest periods of the event [*Mandea-Alexandrescu et al.*, 1999] and (2) the time of the event can be somewhat different in different observatories; for example, in 1969 and 1978, the Southern Hemisphere lags the northern one by some 2 years [*Alexandrescu et al.*, 1996]. We have reported the times of the 20th century jerks, with their uncertainties, on Figure 4. It seems to us again that it is not so far-fetched to propose a correlation between the sequence of these events and the sequence of accidents in the phase of the Chandler wobble. We interpret the jerks as marking changes in the flow at the top of the core responsible for the secular variation [*Gibert et al.*, 1998; *Le Huy et al.*, 2000; *Bellanger et al.*, 2001]. Other interpretations have been proposed, for example, that the jerks can be explained by a core flow consisting of steady motion and torsional oscillations [*Bloxham et al.*, 2002].

[32] But in this paper we focus on the spectacular phase change of $\sim 3\pi/2$ which corresponds to a decrease of the apparent Chandler period of 23 days (equation (3)) from 1926 to 1942 [*Danjon and Guinot*, 1954], and which follows the 1926 magnetic jerk. As far as we know, this large variation has never been convincingly explained by an external forcing, including the atmosphere and/or the ocean, nor by an unusual series of big earthquakes. If external or superficial causes fail to provide the right mechanism, it is reasonable to call for deep sources, i.e., interactions with the core, which is a big reservoir of angular momentum. That is why we are motivated to look for the exchanges of angular momentum between the core and the mantle as a possible cause for these large phase changes, to some extent independently of the suggested coincidence of magnetic jerks with wobble phase changes.

[33] The difficulty is that we need big enough core-mantle torques with short time constants are needed. More precisely, torques of the order of 10^{21} N.m with a duration shorter than 430 days, frequent enough, and which do not cancel each other, are requested. In some previous papers [*Hinderer et al.*, 1987, 1990; *Bellanger et al.*, 2001] we called for the geostrophic torque resulting from the pressure p associated with the geostrophic flow $\vec{u}$ at the top of the core, acting on the large-scale bumps of the CMB [*Jault and Le Mouël*, 1989; *Hide*, 1969] to explain slow irregularities in the drift of the Earth's mean pole with time constants of a few tens of years. But the difficulty with the excitation of the Chandler wobble is, as said above, the need for a dense sequence of short torques which, however, do not lead to unacceptable velocity field $\vec{u}$. This requirement practically rules out the topographic torque [*Jault and Le Mouël*, 1993], taken in the sense given above. Recently, however, it was proposed [*Narteau et al.*, 2001] that the CMB, in addition to the large-scale topography dynamically sustained by the mantle convection, might present a small-scale roughness, with typical length scales ranging from a meter to hundreds of meters, due to physical-chemical

interactions between the core and the mantle. A torque between the core and the mantle then results from the mantle topography displacing volumes of core fluid, some kind of turbulent viscosity coupling, when there is a relative motion $\vec{u}$ between the two envelopes. This torque happens to be proportional to $||\vec{u}||^2$ [*Le Mouël et al.*, 2006]. Without changing significantly the parameters adopted in the latter paper, it is possible, although difficult, to meet the requirements stated at the beginning of this paragraph for the observed 1926 phase change; this phase change does exist and has not received, to our knowledge, any other convincing explanation. In this view, geomagnetic jerks mark changes in the top core flow characteristics and, as a consequence, in the torque exerted by the core on the mantle and conversely. We are currently developing this analysis, its fair to say that the subject is not free of uncertainties.

[34] **Acknowledgments.** The data analyzed in this study were provided by the International Earth Reference Service (http://www.iers.org). Associate Editor Giorgio Spada and referees Mathieu Dumberry, Richard Gross, and Jon Mound made very constructive comments on a first draft of this paper. This study is IPGP contribution 2400.

References

Alexandrescu, M., D. Gibert, G. Hulot, J.-L. Le Mouël, and G. Saracco (1995), Detection of geomagnetic jerks using wavelet analysis, *J. Geophys. Res.*, *100*, 12,557–12,572.

Alexandrescu, M., D. Gibert, G. Hulot, J.-L. Le Mouël, and G. Saracco (1996), Worldwide wavelet analysis of geomagnetic jerks, *J. Geophys. Res.*, *101*, 21,975–21,994.

Aoyama, Y., and I. Naito (2001), Atmospheric excitation of the Chandler wobble, 1983–1998, *J. Geophys. Res.*, *106*, 8941–8954.

Bellanger, E., J.-L. Le Mouël, M. Mandea, and S. Labrosse (2001), Chandler wobble and geomagnetic jerks, *Phys. Earth Planet. Inter.*, *124*, 95–103.

Bellanger, E., D. Gibert, and J. Le Mouël (2002), A geomagnetic triggering of Chandler wobble phase jumps?, *Geophys. Res. Lett.*, *29*(7), 1124, doi:10.1029/2001GL014253.

Bhanot, G. (1988), The Metropolis algorithm, *Rep. Prog. Phys.*, *51*, 429–457.

Bloxham, J., S. Zatman, and M. Dumberry (2002), The origin of geomagnetic jerks, *Nature*, *420*, 65–68, doi:10.1038/nature01134.

Brzeziński, A., and J. Nastula (2002), Oceanic excitation of the Chandler wobble, *Adv. Space Res.*, *30*, 195–200, doi:10.1016/S0273-1177(02)00284-3.

Cazenave, A., and K. Feigl (1994), *Formes et Mouvements de la Terre*, 160 pp., Belin CNRS, Paris.

Chandler, S. C. (1891a), On the variation of latitude: I, *Astron. J.*, *11*, 59–61.

Chandler, S. C. (1891b), On the variation of latitude: II, *Astron. J.*, *12*, 65–70.

Danjon, A., and B. Guinot (1954), Sur une singularité au mouvement des pôles terrestres survenue en 1926, *C. R. Acad. Sci.*, *238*, 1081–1083.

Dehant, V., and O. de Viron (2002), Earth rotation as an interdisciplinary topic shared by astronomers, geodesists and geophysicists, *Adv. Space Res.*, *30*, 163–173, doi:10.1016/S0273-1177(02)00281-8.

De Michelis, P., and R. Tozzi (2005), A local intermittency measure (LIM) approach to the detection of geomagnetic jerks, *Earth and Planet. Sci. Lett.*, *235*, 261–272, doi:10.1016/j.epsl.2005.04.001.

Dickman, S. R. (1993), Dynamic ocean-tide effects on Earth's rotation, *Geophys. J. Int.*, *112*, 448–470.

Gibert, D., and J. Virieux (1991), Electromagnetic imaging and simulated annealing, *J. Geophys. Res.*, *96*, 8057–8067.

Gibert, D., M. Holschneider, and J.-L. Le Mouël (1998), Wavelet analysis of the Chandler wobble, *J. Geophys. Res.*, *103*, 27,069–27,089.

Gross, R. S. (1986), The influence of earthquakes on the Chandler wobble during 1977–1983, *Geophys. J. R. Astron. Soc.*, *85*, 161–177.

Gross, R. S. (2000), The Excitation of the Chandler wobble, *Geophys. Res. Lett.*, *27*, 2329–2332.

Gross, R. S., and J. Vondrák (1999), Astrometric and Space-Geodetic Observations of Polar Wander, *Geophys. Res. Lett.*, *26*, 2085–2088.

Gross, R. S., I. Fukumori, and D. Menemenlis (2003), Atmospheric and oceanic excitation of the Earth's wobbles during 1980–2000, *J. Geophys. Res.*, *108*(B8), 2370, doi:10.1029/2002JB002143.

Guinot, B. (1972), The Chandlerian wobble from 1900 to 1970, *Astron. Astrophys.*, *84*, 207–214.

Hide, R. (1969), Interaction between the Earth's liquid core and solid mantle, *Nature*, *222*, 1055–1056.

Hinderer, J., C. Gire, H. Legros, and J.-L. Le Mouël (1987), Geomagnetic secular variation, core motions and implications for the Earth's wobble, *Phys. Earth Planet. Inter.*, *49*, 121–132.

Hinderer, J., D. Jault, H. Legros, and J.-L. Le Mouël (1990), Core-mantle topographic torque: A spherical harmonic approach and implications for the excitation of the Earth's rotation by core motion, *Phys. Earth Planet. Inter.*, *59*, 329–341.

Jault, D., and J.-L. Le Mouël (1989), The topographic torque associated with a tangential geostrophic motion at the core surface and inferences on the flow inside the core, *Geophys. Astrophys. Fluid Dyn.*, *48*, 273–296.

Jault, D., and J.-L. Le Mouël (1993), Circulation in the liquid core and coupling with the mantle, *Adv. Space. Res.*, *13*, 221–233, doi:10.1016/0273-1177(93)90225-Z.

Kirkpatrick, S., C. D. Gelatt, and M. P. Vecchi (1983), Optimization by simulated annealing, *Science*, *220*, 671–680.

Lambeck, K. (1980), *The Earth's Variable Rotation*, 449 pp., Cambridge Univ. Press, New York.

Le Huy, M., M. Mandea, J.-L. Le Mouël, and A. Pais (2000), Time evolution of the fluid flow at the top of the core, geomagnetic jerks, *Earth Planet. Space*, *52*, 163–173.

Le Mouël, J. L., C. Narteau, M. Greff-Lefftz, and M. Holschneider (2006), Dissipation at the core-mantle boundary on a small-scale topography, *J. Geophys. Res.*, *111*, B04413, doi:10.1029/2005JB003846.

Macmillan, S. (1996), A geomagnetic jerk for the early 1990's, *Earth Planet. Sci. Lett.*, *137*, 189–192.

Mandea-Alexandrescu, M., D. Gibert, J.-L. Le Mouël, G. Hulot, and G. Saracco (1999), An estimate of average lower mantle conductivity by wavelet analysis of geomagnetic jerks, *J. Geophys. Res.*, *104*, 17,735–17,745.

Mansinha, L., and D. E. Smylie (1967), Effect of earthquakes on the Chandler wobble and the secular polar shift, *J. Geophys. Res.*, *72*, 4731–4743.

Metropolis, N., A. Rosenbluth, N. Rosenbluth, A. Teller, and E. Teller (1953), Equation of state calculations by fast computing machines, *J. Chem. Phys.*, *21*, 1087–1092.

Mosegaard, K. (1998), Resolution analysis of general inverse problems through inverse Monte Carlo sampling, *Inverse Problems*, *14*, 405–426.

Mosegaard, K., and A. Tarantola (1995), Monte Carlo sampling of solutions to inverse problems, *J. Geophys. Res.*, *100*, 12,431–12,447.

Narteau, C., J. L. Le Mouël, J.-P. Poirier, E. Sepúlveda, and M. G. Shnirman (2001), On a small scale roughness of the core-mantle boundary, *Phys. Earth Planet. Inter.*, *191*, 49–61.

Pessel, M., and D. Gibert (2003), Multiscale electrical impedance tomography, *J. Geophys. Res.*, *108*(B1), 2054, doi:10.1029/2001JB000233.

Sambridge, M., and K. Mosegaard (2002), Monte Carlo methods in geophysical inverse problems, *Rev. Geophys.*, *40*(3), 1009, doi:10.1029/2000RG000089.

Shirai, T., T. Fukushima, and Z. Malkin (2005), Detection of phase disturbances of free core nutation of the Earth and their concurrence with geomagnetic jerks, *Earth Planets Space*, *57*, 151–155.

Wahr, J. (1988), The Earth's rotation, *Annu. Rev. Earth Planet. Sci.*, *16*, 231–249.

D. Gibert and J.-L. Le Mouël, Institut de Physique du Globe de Paris, 4 place Jussieu, F-75252 Paris, CEDEX 05, France. (gibert@ipgp.fr; lemouel@ipgp.fr)